Insights About the Influence of the Refractory Purging Device on the Kinetics of Nonmetallic Inclusion Removal in Steelmaking

Falsetti, Luís Otávio Z.; Charruault, Florian; Delfos, René; Luchini, Bruno; van der Plas, Dirk; Pandolfelli, Victor C.

DOI
10.33313/389/106

Publication date
2025

Document Version
Final published version

Published in
Proceedings of the Iron and Steel Technology Conference, AISTech 2025

AISTech 2025 — Proceedings of the Iron & Steel Technology Conference
5–8 May 2025, Nashville, Tenn., USA
DOI: 10.33313/389/106

Insights About the Influence of the Refractory Purging Device on the Kinetics of Nonmetallic Inclusion Removal in Steelmaking

Luís Otávio Z. Falsetti[1], Florian Charruault[2], René Delfos[3], Bruno Luchini[2], Dirk van der Plas[2], Victor C. Pandolfelli[1]

[1]Federal University of São Carlos (UFSCar), Graduate Program in Materials Science and Engineering (PPGCEM)
Materials Microstructure Engineering Group (GEMM), FIRE Associate Laboratory
Rod. Washington Luís km 235 (SP-310), São Carlos, SP, Brazil, 13565-905
Phone: +55 (16) 3351-8111
Email: luisotavio@dema.ufscar.br, vicpando@ufscar.br

[2]Tata Steel Nederland, Research & Development, IJmuiden Technology Centre
PO Box 10000, Ijmuiden, South Holland, the Netherlands, 1970 CA
Phone: +31 (0) 251 4 98047
Email: florian.charruault@tatasteeleurope.com, bruno.luchini@tatasteeleurope.com, dirk.van-der-plas@tatasteeleurope.com

[3]Laboratory for Aero and Hydrodynamics, Delft University of Technology
Mekelweg 2, Delft, South Holland, the Netherlands, 2628 CD
Phone: +31 (0) 15 27 89809
Email: r.delfos@tudelft.nl

ABSTRACT

Beyond metallurgical aspects to yield clean steels, purging plugs in the ladle and beams in the tundish play a key role in generating bubble curtains to maximize the nonmetallic inclusion removal in a short time. However, technical challenges might be noted on how to control the bubble size through the design of the purging device and how to predict the kinetics of induced flotation for each bubble plume. Therefore, this work investigated two bubble size distributions and their effect on the kinetics of particle removal in a water model, providing insights into the design of purging devices for clean steelmaking.

Keywords: Clean steel, Non-metallic inclusion, Porous brick, Purging beam, Tundish purging

INTRODUCTION

Various sources of non-metallic inclusions might be identified throughout the refining of liquid metal. Whereas some can be lessened by properly installing flow control devices and adjusting the slag and mold powder's chemical composition [1,2], others are inherent to the steelmaking process – namely, the contact with ceramic refractories and the deoxidation of liquid metal (generating oxide inclusions), making the removal of non-metallic a recurrent challenge for metallurgists. Consequently, injecting inert gas bubbles is crucial to the induced flotation of inclusions, speeding up the refining of the liquid metal. The injection of inert gas bubbles in the liquid metal provides additional mechanisms of induced flotation by which inclusions may be removed: (i) attachment to the bubble surface, according to the probabilities of collision, adhesion and detachment [3]; (ii) captured in the bubble´s wake zone, after entering the rising zone [4]; (iii) carried by the flow pattern caused by the bubble plume [5]. Collecting the flotation mechanisms, complexity can be observed in determining the optimum conditions to effectively withdraw non-metallic inclusions from liquid metal, yielding clean steel grades. Even so, efforts to define the optimum bubble size range were made based on the total probability of inclusion removal by bubble attachment, i.e. mechanisms "(i)", mentioned above. According to Wang et al. [6], the likelihood of collision and adhesion are maximized when bubbles are smaller than 2.0 mm, whereas the detachment probability increases for bubbles below 0.5 mm. Thus, an optimum bubble size range between 0.5 and 2.0 mm is typically pursued for ceramic refractory devices aiming at steel cleanliness.

With these concepts in mind, the goal of producing "clean steels" turns into a challenge to the design of porous ceramic refractories to fulfil the requirement of bubble sizes within the optimum range. Previous studies from the authors have shown the importance of the plug's surface wettability in generating bubbles, where high contact angles with the liquid cause the bubble to spread over the bubbler, increasing its equilibrium diameter for detachment [7]. Under these conditions, the effect of the pore diameter on the bubble size might even be hindered. On the other hand, designing a porous structure with a low contact angle (highly wettable) and larger pore size to also allow the injection of low-to-high gas flow rates is not a good alternative when aiming at controlling the infiltration of liquid metal, as the only controllable variable would be the gas counterpressure [8]. In this scenario, the tundish allows a constant injection of gas along its life span, reducing the infiltration of liquid metal and even making the application of wettable compositions possible. Besides, there is no requirement for high gas flow rates as alloying is not conducted in the tundish and, thus, a porous structure may be designed focusing on inclusion removal. Commercial solutions for injecting gas in the tundish are currently available, consisting of magnesia porous bricks operating with gas flow rates of 10 to 60 NL/min [9].

Focusing on the influence of the bubble size distribution and gas flow rate on the kinetics of particle's flotation, the authors conducted experiments on a water model with two porous structures to generate a bubble plume in a quasi-2D recirculating water tank. Hydrophobic glass hollow particles were applied to simulate the behavior of non-metallic inclusions, and their concentration was indirectly measured by light scattering and fitted by an exponential decay. Unlike other works from the literature [10–12], the aim of the present one is not to reproduce a specific industrial tundish setup, but to gain experimental insights into the influence of the bubble plume on the efficiency and characteristic time for the removal of NMIs.

METHODOLOGY

The physical simulations of induced flotation were conducted in a water model with a 1000 x 400 x 40 mm³ vessel, filled with softened tap water and coupled with a system to homogenize the concentration of particles during the experiment (Fig. 1a). The behavior of non-metallic inclusions was reproduced by glass hollow spheres (Potters Q-Cel 7014) as in Fig. 1b, following a procedure to sieve them to a size distribution between 10.1 and 64.3 μm (d10 and d90, respectively). The nature of these particles provided the indirect measurement of their concentration using a light scattering method, where a scientific camera (LaVision VC-Imager sCMOS CLHS) recorded the scattered rays at 2 Hz and an exposure time of 1 ms. The experiment consisted of (a) 5 minutes of homogenization after injecting 80 mL of the particle suspension, (b) 10 minutes of natural flotation - without injecting gas, (c) 25 minutes of combined flotation - when the mechanisms induced by the bubble plume were coupled, and (d) a step of filtering out particles to ensure that the background did not change throughout the measurement. More details of the experimental setup are available in a previous publication by the authors [13]. The light intensity along the steps of flotation ("b" and "c") was fitted by an exponential decay function over time (t), as in Eq. 1, from which the time scale (TS) is directly obtained. The final efficiency is calculated as $Eff = \frac{I_\infty}{I_\delta + I_\infty}$, where I_∞ and I_δ represent the intensity at an infinity time and the decrease from the initial value, respectively.

$$I(t) = I_\delta \cdot \exp(TS^{-1} \cdot t) + I_\infty \quad (1)$$

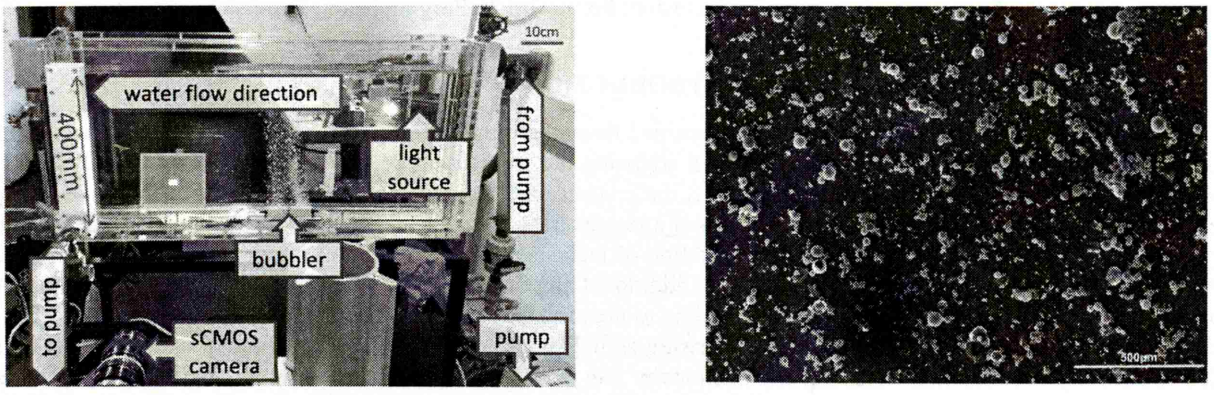

(a) (b)

Fig. 1: (a) Front view of the water model and the coupled devices and (b) micrograph of the glass particles after the sieving procedure. Extracted from [13].

Industrially speaking, the gas injection in the tundish is typically controlled in the normal liter per minute (NL/min). However, the actual volume of gas released by the porous structure is affected by temperature and pressure differences from the standard conditions, and by the area of the porous bubbler. Thus, by applying this assumption when using purging beams, the

corresponding value in L/min/m² may be obtained, representing the volume of gas injected per square meter - also referred to as the linear velocity of the gas at the outlet, as the dimensional analysis of the units will lead to "Length/Time". To carry out this procedure, the standard flow rate is converted to the actual gas flow rate on the porous surface, by assuming an ideal gas behavior and considering the temperature and pressure difference from the standard conditions (T_{std} and P_{std}, respectively) to those at the gas outlet (T_{gas} and P_{gas}). Assuming a 1m-high column in the tundish (H_l) of liquid steel with a density of 7000 kg/m³ (ρ_l), the linear velocity of the gas (U_g) is derived by Eq. 2, where "A_{PB}" is the area of the purging beam and "g" the gravitational acceleration.

$$U_g = Q_{g,std} \cdot \frac{101325\ Pa}{273K} \cdot \frac{573K}{101325\ Pa + \rho_l\ g\ H_l} \cdot \frac{1}{A_{PB}} \tag{2}$$

As mentioned in the Introduction section, the typical range for the gas flow rate in a purging beam of 900 x 100 mm² is within 10 to 60 NL/min. Substituting these values into Eq. 2, the corresponding gas flow rate per area is expected within the 140 to 830 L/min/m² range. To simulate this condition in the water model, two kinds of porous structures were applied: a pair of commercial air diffusers (AD) and a porous ceramic brick (PB). The gas flow rate injected through these bubblers was measured by a calibrated flow meter in the range of 25 to 250 L/h. The correlation between the gas flow rate applied to the purging beam in the tundish and to the bubbler in the water model is summarized in Fig. 2, highlighting that the experimental conditions of the conducted tests are within the industrial range - except for experiment "B1", which falls below the lower limit.

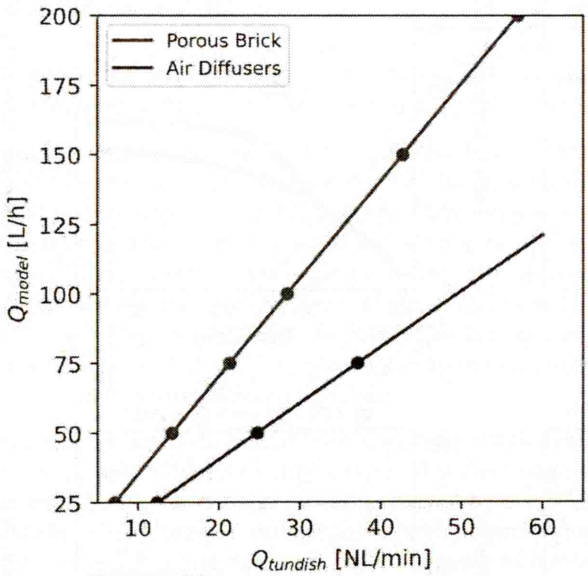

Fig. 2: Correlation between gas flow rates of industrial tundishes (in NL/min) and the corresponding value in the water model (in L/h), by keeping "U_g" constant according to Eq. 2.

The bubble plumes for the six flow rates were characterized by a shadowgraphy technique, where an LED panel (9x16 in², roughly 23x41 cm², from Edmund Optics) was placed behind the water model and the sCMOS camera captured the shadow generated by the bubbles [14]. The recorded frames were analyzed by an algorithm in Python using the OpenCV library (cv2). In general, the air diffusers generate an average bubble of 0.6 mm (0.2 - 1.4mm), whereas the porous brick produces 1.1 mm bubbles (0.7 - 1.6mm), despite of the gas flow rate. Compared to the optimum size range described in the literature (0.5 - 2.0mm), the porous brick generated bubbles within the suggested limits, whereas the air diffusers were closer to the lower limit.

RESULTS AND DISCUSSION

The particle removal as a function of time for the natural and induced flotation was recorded, and the results are presented in Fig. 3. Considering that the nine experiments began with a natural flotation step, there is a similar pattern in the first 10 minutes after the homogenisation of particles in the system, as no gas is being injected yet. From the moment when the porous structure is blown with compressed air, some bubbles reach the camera's field of view, scattering light and causing the particle removal to be artificially decreased for a while. These bubbles float right away and this effect does not disturb the subsequent results as the bubble plume is already developed. From 10 to 35 minutes, the results represent the combination of natural and induced flotation mechanisms, as bubbles now also help the removal of particles. Comparing the fitted blue curves for the nine conditions, various removal rates and efficiencies are expected.

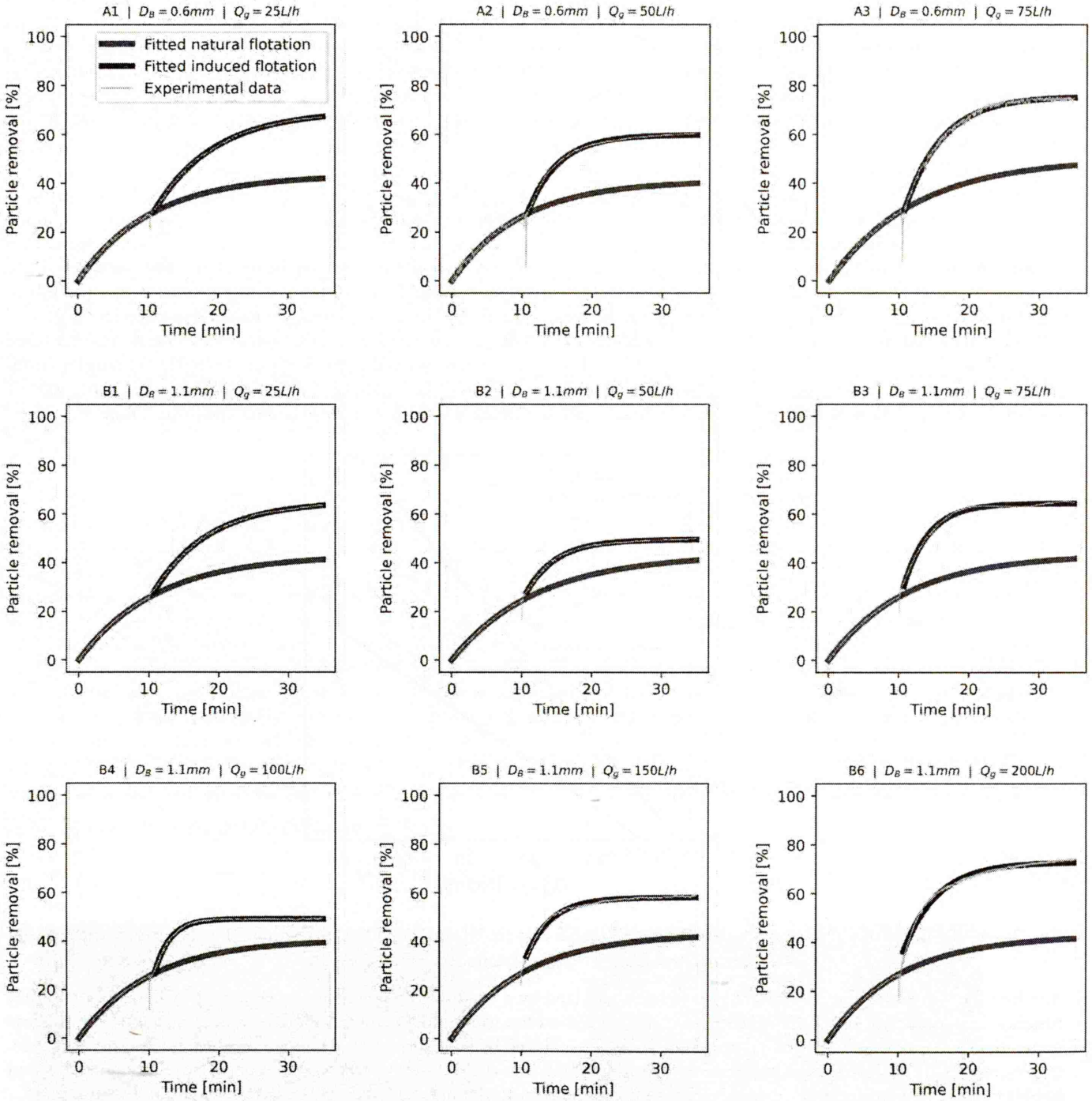

Fig. 3: Percentage of particle removal as a function of time presenting the fitted natural flotation (dark red line) and induced one (dark blue line) for the various gas flowrate [15].

An exponential decay fitted the light intensity data for the natural and induced flotation, and the parameters of time scale and maximum efficiency for each experiment are summarized in Fig. 4 and Fig. 5. The average value for the parameters of natural flotation was a time scale of 650 ± 41s and a maximum efficiency of 42.8 ± 1.0%, with a coefficient of variation of 6.3% and 2.3%, respectively. These values attest the reproducibility of the experiment's initial conditions (before the bubble plume is injected), providing a direct comparison among the results for induced flotation. Besides, it is worth noticing that although the average efficiency is 42.8%, this value represents an extrapolation at an infinity time, whereas the system has roughly three-quarters of the initial particle concentration still in suspension after the 10 minutes of natural flotation, thus allowing the analysis of the share of induced mechanisms to flotation.

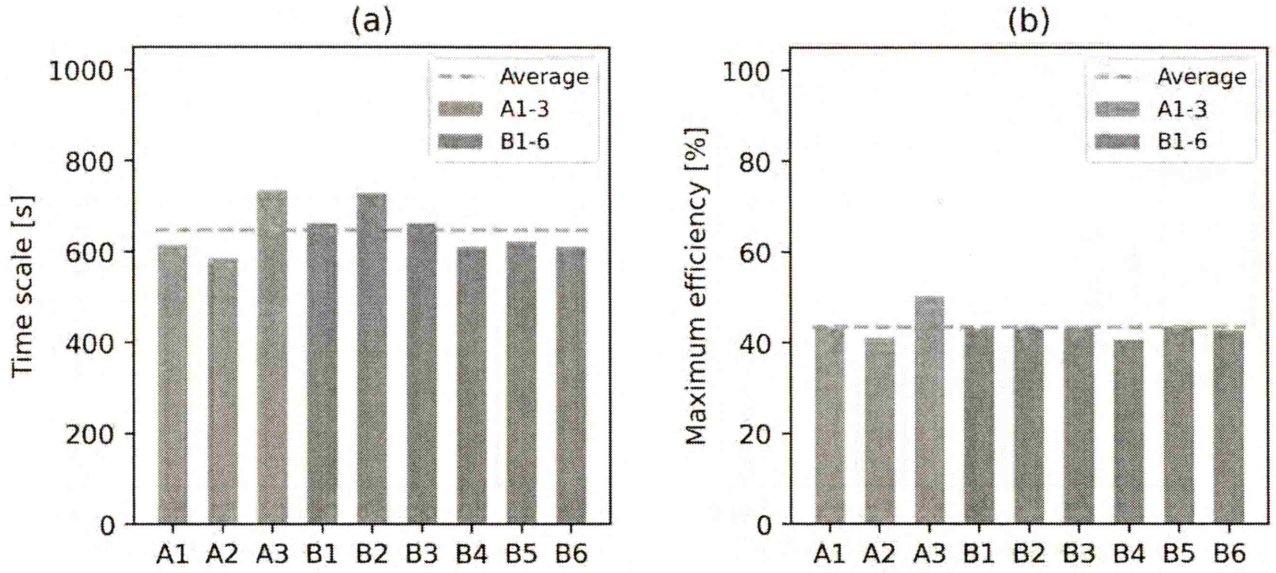

Fig. 4: The collected (a) time scales and (b) maximum efficiencies for the experiments considering only the natural flotation, highlighting the reproducibility of the experiment's initial condition [15].

The time scale and maximum efficiency values comprising the share of induced flotation mechanisms are shown in Fig. 5 and plotted as a function of the gas flow rate per area (U_g). The averages for the plain natural flotation are also indicated to ease the values' comparison (grey dashed line), highlighting a noticeable decrease in the time scale when the bubble plume is injected, regardless of the gas flow rate. Moreover, the trend seems to be of a U-shaped profile in Fig. 5a, suggesting an optimal gas flow rate to speed up the particle flotation. The initial decrease in time scale is in tune with other experiments from the literature, where an increase in the gas flow rate caused a higher particle removal rate (i.e., lower TS), even though their authors did not correlate it to a specific flotation mechanism [16–18]. However, by increasing the gas flow rate even further, the removal rate tends to decrease. The complete behavior may be analyzed considering the three mechanisms of flotation induced by bubbles: (i) surface attachment, (ii) wake capture and (iii) flow-induced removal.

Even though the effect of the gas flow rate on the likelihood of bubble-particle attachment and volume of bubble wake region is typically discussed in the literature for a single bubble, one might expect that their magnitudes are proportional to the number of bubbles in the plume. Thus, as the bubble size was not significantly affected by the gas injection in this work, a higher flow rate should induce mechanisms (i) and (ii) (particle attachment and bubble wake capture, respectively), leading to a proportional increase in the removal rate. However, it is worth comparing the marginal increase of removal rate when the gas flow rate rises from 95 to 190 L/min/m² (90% faster, for 1.1 mm bubbles) and from 190 to 380 L/min/m² (72% faster), as the latter is less noticeable. This effect is likely because the collision probability and the wake region of an individual bubble are affected by the neighboring bubbles in the plume, not representing a simple addition of the shares from each one. Besides, when increasing the gas flow rate even further, from 380 to 770 L/min/m² for 1.1 mm bubbles, an increase in the time scale is seen in Fig. 5a, indicating a lower removal rate. A first hypothesis on the reason behind this effect could be the recirculation pattern induced by the bubble plume, whose velocity scales with the cubic root of the gas flow rate, according to the literature [19]. By mass conservation, the velocity of the ascending plume scales with the horizontal flow velocity on the top region of the model, which reduces the time for the floated particle to be transferred to the liquid's free surface. However, the recordings of the bubble plumes at 50Hz during the experiments show that the vertical velocities are similar – for instance, 291 and 273 mm/s for 50 and 200 L/h, respectively, and 1.1 mm bubbles. Consequently, as the bubble size remains the same, a higher gas flow rate leads to more bubbles per volume for a constant residence time of the plume in the system. Another hypothesis is that a larger number of bubbles reaching the system's free surface per unit of time causes higher turbulence, disturbing the transfer of the particle to this top layer. If so, it could not be investigated further with the current setup. Overall, although an increase in the gas flow rate is beneficial to the induced mechanisms of flotation [3,4], it might spoil the removal rates at high values.

Analyzing Fig. 5b, smaller bubbles (0.6mm) were able to remove more particles in suspension, leading to higher efficiencies. However, there is no clear trend for this parameter as a function of the gas flow rate. Thus, clustering the results by bubble size (dashed lines), the average efficiency was calculated as 68.4 ± 6.5% for 0.6 mm bubbles and 59.8 ± 7.3% for 1.1mm ones. When compared to the average efficiency of natural flotation (44.1%), the bubble plume's share removal of hydrophobic particles is noticeable.

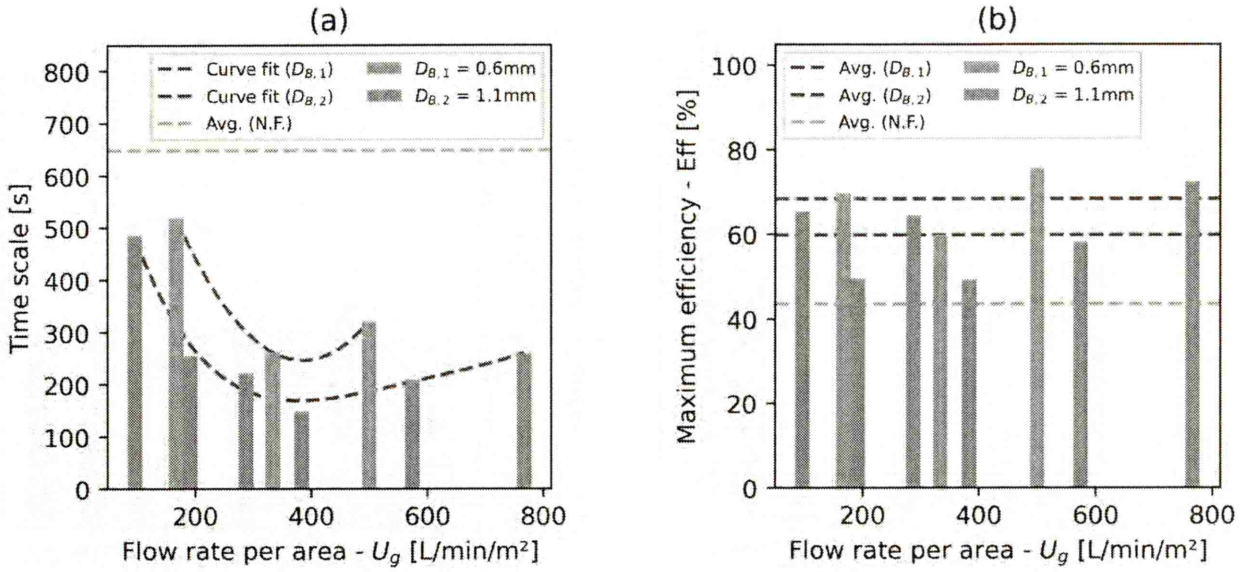

Fig. 5: The collected (a) time scales and (b) efficiencies for the nine experiments considering both the natural and induced flotation, comparing the results to the average of plain natural flotation (grey dashed lines) [15].

INSIGHTS INTO THE INDUSTRIAL PRACTICE

The question now raised is "What can we learn from the results and how to apply them to the practice of bubbling in the tundish to remove the maximum number of inclusions?". Firstly, compared to the results for plain natural flotation (Fig. 4), the injection of gas decreases the required time for particle flotation (TS) and increases the maximum efficiency that could be attained. However, some parameters can be adjusted when installing a bubble curtain in the tundish: the gas flow rate, the bubbler area and the target bubble size. Starting from the gas flow rate, the results suggest an optimum value for which the time scale would be the lowest. In the case of the current experiments, this condition was attained at around 300 to 500 L/min/m² for both bubble sizes. As this model was not designed specifically to reproduce an industrial tundish, some considerations might be expected to determine this condition for a certain steelmaking plant. According to Sahai and Emi [10], the similarity of Reynolds' and Froude's criteria could only be simultaneously satisfied when the water model has the same dimensions as the industrial vessel. Thus, the optimum range of U_g (300-500 L/min/m²) defined in the present work could only be related to relatively shallow tundishes and converted to industrial gas flow rates of 20 to 35 NL/min when considering the commercial "purging beam". This gas flow rate could also be a starting point for other industrial setups, although specific water models would be required to get more insights.

Even though there was no clear trend between the maximum efficiency of removal and the gas flow rate, it is important to remember that this value represents an extrapolation at an infinite time. For example, this condition could be attained in a ladle by increasing the bubbling time, as the molten bath recirculates in this vessel. However, the tundish works as a buffer and the tools to increase the residence time of the liquid metal in this vessel are limited to flow modifiers (such as dams and weirs). Therefore, it is crucial to have high removal rates (i.e., low time scale) to ensure maximum cleanliness of the liquid metal in a short time. Alternatively, a higher number of bubble curtains can be installed in the tundish, or a larger area covered by the porous bricks, increasing the interaction time between the liquid metal and the bubble plume while remaining within the optimum range for U_g.

In order to illustrate it, Fig. 6 presents a calculated scenario for 0.6 and 1.1mm bubbles, comparing their performance as a function of the number of interactions with the bubble plume. First, Fig. 5a has been considered to define the optimum Time Scale close to 385 L/min/m² and, coupled to the mean maximum efficiency from Fig. 5b, the particle removal across time was determined. Besides, the recirculation time in the water model was estimated to be close to 50 seconds, which could be correlated to a single pass in the tundish. Having this information in mind, Fig. 6 shows that a single pass through the bubble curtain removes 12.6% of particles when 0.6mm bubbles are applied, while 15.3% are removed when the bubble has a 1.1mm diameter. For two passes, these values increase to 22.8% and 26.7%, respectively, achieving 43.6% and 46.2% after five passes. Interestingly, it takes seven passes for both bubble plumes' performance to be the same, from when the 0.6mm bubbles begin to remove more particles than the 1.1mm ones.

In order to illustrate it, Fig. 6 presents a calculated scenario for 0.6 and 1.1mm bubbles, comparing their performance as a function of the number of interactions with the bubble plume. Considering that Fig. 5a defines an optimum value for the gas

flow rate close to 385 L/min/m², the expected Time Scales would be 247 and 169 s for 0.6 and 1.1mm bubbles, respectively. Coupled with the mean maximum efficiency from Fig. 5b, the particle removal across time was determined by the exponential decay function (Eq. 2). Besides, the recirculation time in the water model was estimated to be close to 50 second, which is in tune with the estimated value of 47 seconds considering the model's volume of 17 L (including 5 L for the tubing) and the recirculation rate of 21.6 L/min. This period could be correlated to a single pass through a bubble plume in the tundish. Having this information in mind, Fig. 6 shows that a single pass removes 12.6% of particles when 0.6mm bubbles are applied, while 15.3% are removed when the bubble has a 1.1mm diameter. For two passes, these values increase to 22.8% and 26.7%, respectively, achieving 43.6% and 46.2% after five passes. Interestingly, it takes seven passes for both bubble plumes' performance to be the same, from when the 0.6mm bubbles begin to remove more particles than the 1.1mm ones. Due to the exponential behavior of particle removal, it takes 5-6 passes for the 1.1mm bubbles to remove 80% of its maximum efficiency, but 10 passes to remove 95%.

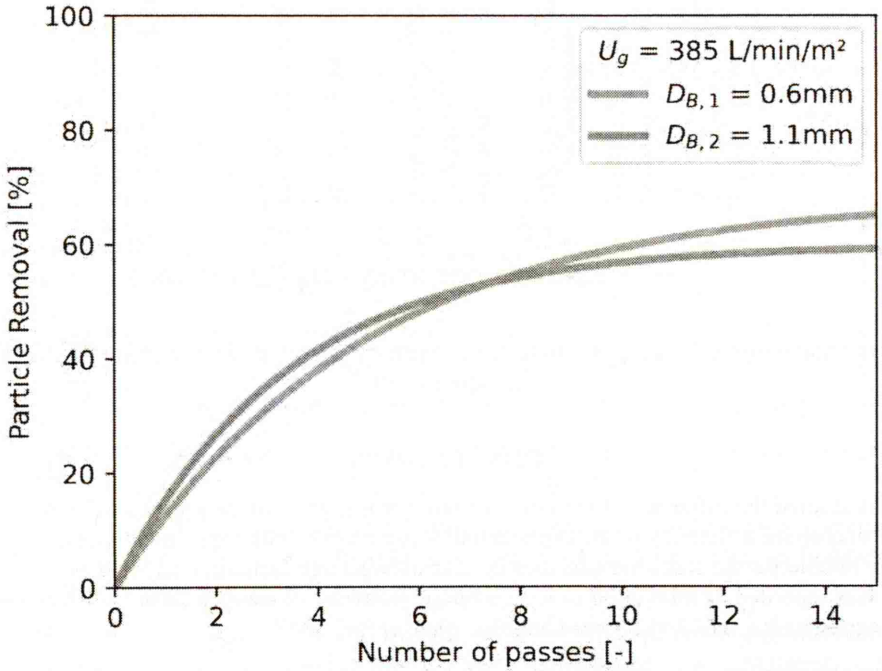

Fig. 6: Calculated scenario for particle removal at the optimum gas flow rate (385 L/min/m²) as a function of the number of passes through the bubble plume.

Complementarily, one must remember that the current setup of the water model applies a recirculating flow of particle suspension. Thus, the removal rate at the first moments of gas injection better represents the interaction with the bubble plume in the tundish, and higher values would mean a more effective purging device for a given gas flow rate. Following this idea, Eq. 3 is obtained by taking the derivative of the exponential decay in Eq. 1 and evaluating the removal rate at t = 0.

$$\left.\frac{dI}{dt}\right|_{t=0} = -(I_o - I_\infty) \cdot \frac{1}{TS} \tag{3}$$

By taking a close look on Eq. 3 and considering that the light intensity is normalized between 0 and 100% for the flotation experiments, the first term is given as the initial intensity (I_o = 100%) minus the percentage at an infinite time (I_∞), which represents the maximum removal efficiency. In other words, Eq. 3 is directly proportional to the ratio between Efficiency and Time Scale, allowing Fig. 7 to be obtained which compares the various gas flow rates and bubble diameters. From this result, the highest initial removal rate was obtained at 380 L/min/m² for 1.1mm bubbles, and at 500 L/min/m² for 0.6mm bubbles. However, the removal rate at this latter condition is still 29% lower, meaning that less particles would be removed at a single pass through the bubble plume.

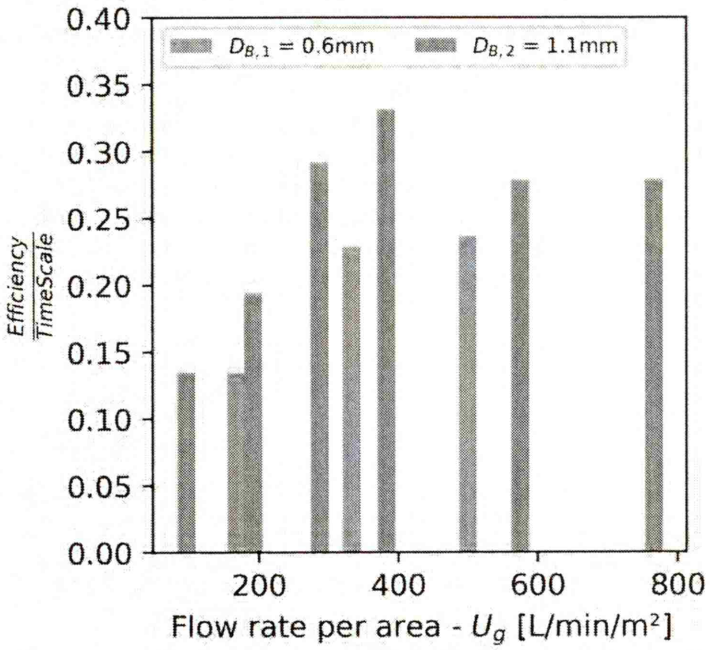

Fig. 7: The ratio between maximum efficiency and time scale, representing the initial removal rate, for the various conditions of experiments.

CONCLUSIONS

In this work, the authors studied the influence of the gas flow rate per unit area on the kinetics of particle removal, considering the time scale and the maximum efficiency of an exponential decay profile. The experiments were conducted in a quasi-2D water model where the bubble plume was characterized by a shadowgraphy technique coupled with image analysis, and the particle concentration was recorded as a function of time by light scattering. Two distinct size distributions of bubble plumes were generated in the experiments: 0.6- and 1.1-mm bubbles, on average.

The results indicated an optimum gas flow rate for which the time scale was the lowest, leading to faster removal rates. This behaviour of a U-shaped curve was correlated to the mechanisms of bubble-induced flotation. On the other hand, as the maximum efficiency represents an extrapolation of the exponential decay at an infinite time, there was no clear trend of this parameter as a function of the gas flow rate. In summary, this value increased from 44.1% for the plain natural flotation to 68.4 and 59.8 %, for 0.6 and 1.1mm bubbles, respectively. On the other hand, the smaller bubbles led to a higher time scale (slower removal rate). Therefore, a trade-off between removing more inclusions and attaining this condition in a shorter time is defined by the bubble size.

Applying these results to the industrial practice in the tundish, the project of a porous brick should consider the number of bubble curtains and the bubbler's coverage area, as longer interaction times with the bubble plume might be required to attain high efficiencies. To illustrate it, although smaller bubbles (0.6mm) led to a higher maximum efficiency, it would take more than 15 passes through the bubble plume for this value to be attained, which seems unfeasible in an industrial tundish. On the other hand, the 1.1mm bubbles displayed a lower time scale, translating into short times to reach the maximum removal efficiency. For this latter bubble plume, the efficiencies at the optimum gas flow rate (385 L/min/m²) were estimated for one, two and five passes in 15.3%, 26.7% and 46.2%. In other words, 80% of the removable particles are floated after 5-6 passes, while 10 passes are required to reach 95%. Thus, the tundish shows great potential to increase the steel's cleanliness but should work together with the porous plug in the ladle to attain low concentrations of inclusions.

ACKNOWLEDGEMENTS

This study was financed in part by the Coordenação de Aperfeiçoamento de Pessoal de Nível Superior - Brasil (CAPES) - Finance Code 001 and by the São Paulo Research Foundation (FAPESP) - grant 2022/00378-2. The authors are also thankful to Bart Hoek, Jasper Ruijgrok and Edwin Overmars for their support with the experimental model and measurement, to RHI-Magnesita for providing details about commercial products, and to FIRE (Federation for International Refractory Research and Education) for supporting this research. The methodology and results are in part based on Falsetti, Charruault, Delfos, Luchini, van der Plas and Pandolfelli's paper published in the International Journal of Applied Ceramic Technology (2025).

REFERENCES

1. W. Yang, L. Zhang, Y. Ren, W. Chen, F. Liu, Formation and prevention of nozzle clogging during the continuous casting of steels: A review, ISIJ International 64 (2024) ISIJINT-2023-376. https://doi.org/10.2355/isijinternational.ISIJINT-2023-376.
2. T.S. Kim, Y. Chung, L. Holappa, J.H. Park, Effect of rice husk ash insulation powder on the reoxidation behavior of molten steel in continuous casting tundish, Metallurgical and Materials Transactions B 48 (2017) 1736–1747. https://doi.org/10.1007/s11663-017-0971-3.
3. L. Zhang, S. Taniguchi, Fundamentals of inclusion removal from liquid steel by bubble flotation, International Materials Reviews 45 (2000) 59–82. https://doi.org/10.1179/095066000101528313.
4. H.L. Yang, P. He, Y.C. Zhai, Removal behavior of inclusions in molten steel by bubble wake flow based on water model experiment, ISIJ International 54 (2014) 578–581. https://doi.org/10.2355/isijinternational.54.578.
5. S. Joo, R.I.L. Guthrie, Modeling flows and mixing in steelmaking ladles designed for single- and dual-plug bubbling operations, Metallurgical Transactions B 23 (1992) 765–778. https://doi.org/10.1007/BF02656455.
6. L. Wang, H.G. Lee, P. Hayes, Prediction of the optimum bubble size for inclusion removal from molten steel by flotation, ISIJ International 36 (1996) 7–16. https://doi.org/10.2355/isijinternational.36.7.
7. L.O.Z. Falsetti, D.N. Ferreira Muche, M.R.B. Andreeta, M.H. Moreira, V.C. Pandolfelli, Bubble generation in refractory porous plugs: The role of the ceramic surface composition, International Journal of Ceramic Engineering and Science 4 (2022) 199–210. https://doi.org/10.1002/ces2.10132.
8. L.O.Z. Falsetti, D.N. Ferreira Muche, V.C. Pandolfelli, Development of porous refractory ceramic plugs: Will the next generation be 3D printed?, Ceram Int 47 (2021) 26350–26356. https://doi.org/10.1016/j.ceramint.2021.06.045.
9. RHI-Magnesita, Beyond refractories - Discover our flow control solutions, (2021). https://www.beyond-refractories.com.
10. Y. Sahai, T. Emi, Criteria for water modeling of melt flow and inclusion removal in continuous casting tundishes, ISIJ International 36 (1996) 1166–1173. https://doi.org/10.2355/isijinternational.36.1166.
11. M.J. Zhang, H.Z. Gu, A. Huang, H.X. Zhu, C.J. Deng, Physical and mathematical modeling of inclusion removal with gas bottom-blowing in continuous casting tundish, Journal of Mining and Metallurgy, Section B: Metallurgy 47 (2011) 37–44. https://doi.org/10.2298/JMMB1101037Z.
12. V. Seshadri, C.A. da Silva, I.A. da Silva, E. da S. Araújo Júnior, A physical modelling study of inclusion removal in tundish using inert gas curtain, Tecnologia Em Metalurgia e Materiais 9 (2012) 22–29. https://doi.org/10.4322/tmm.2012.004.
13. L.O.Z. Falsetti, R. Delfos, F. Charruault, B. Luchini, D. Van Der Plas, V.C. Pandolfelli, Wettability of non-metallic inclusions and its impact on bubble-induced flotation kinetics, Int J Appl Ceram Technol 21 (2024) 3835–3841. https://doi.org/10.1111/ijac.14849.
14. A. Srivastava, A. Asgarian, J. Sengupta, K. Chattopadhyay, Bubble characterization in a continuous casting mold: Comparison and identification of image processing techniques, Metallurgical and Materials Transactions B 53 (2022) 2438–2457. https://doi.org/10.1007/s11663-022-02541-2.
15. L.O.Z. Falsetti, F. Charruault, R. Delfos, B. Luchini, D. van der Plas, V.C. Pandolfelli, Bubble plume effects on the flotation kinetics of non-metallic inclusions based on experimental observations, Int J Appl Ceram Technol 22 (2025) e14972. https://doi.org/10.1111/ijac.14972.
16. L. Zhang, S. Taniguchi, K. Matsumoto, Water model study on inclusion removal from liquid steel by bubble flotation under turbulent conditions, Ironmaking & Steelmaking 29 (2002) 326–336. https://doi.org/10.1179/030192302225007879.
17. Y. Kwon, J. Zhang, H.-G. Lee, Water model and CFD studies of bubble dispersion and inclusions removal in continuous casting mold of steel, ISIJ International 46 (2006) 257–266. https://doi.org/10.2355/isijinternational.46.257.
18. F. Jiang, G.G. Cheng, Inclusion removal at the free surface of steel bath by bubble flotation, Adv Mat Res 399–401 (2011) 216–222. https://doi.org/10.4028/www.scientific.net/AMR.399-401.216.
19. Y. Sahai, R.I.L. Guthrie, Hydrodynamics of gas stirred melts: Part I. Gas/liquid coupling, Metallurgical Transactions B 13 (1982) 193–202. https://doi.org/10.1007/BF02664576.